Astron. Astrophys. 349, 996–1002 (1999)

ASTRONOMY AND ASTROPHYSICS

Photoionization cross sections for Fe XVI and Fe XVII recombination rate coefficients

D. Donnelly, K.L. Bell, W.G.V. Darlington, R.H.G. Reid, and F.P. Keenan

School of Mathematics and Physics, The Queen's University of Belfast, Belfast, BT7 1NN, Northern Ireland

Received 27 January 1999 / Accepted 4 June 1999

Abstract. The Breit-Pauli R-matrix codes are utilized in a detailed study of the photoionization of the ground state of Fe XVI ($2s^2 2p^6 3s\ ^2S_{1/2}$). High resolution total and partial cross sections are obtained using 37 $J\pi$ configuration interaction type wavefunctions to represent the residual ion, Fe XVII, after $3s$, $2p$ and $2s$ photoionization. For the total cross section, the work of Verner et al. and previous Opacity Project calculations are in fair agreement with the present results, while relativistic effects are seen to have a noticeable but not an overly significant effect on the background cross section. The derived partial cross sections are used in a calculation of rates for the recombination of states of Fe XVII to the ground state of Fe XVI.

Key words: atomic data – atomic processes

1. Introduction

Line emission from Fe L-shell ions has been extensively detected in the soft X-ray spectra of coronal plasmas such as the Sun (Phillips et al. 1982), and from accretion-powered sources including active galactic nuclei, cataclysmic variables and X-ray binaries (Liedahl et al. 1995). To date, the diagnostic applications of Fe L-shell spectra have been primarily restricted to the solar corona (see, for example, Keenan 1996 and references therein), due to the availability of high spectral resolution observations. By contrast, current data for cosmic X-ray sources (provided for example by the BBXRT and ASCA satellites; Yaqoob et al. 1995; Audley et al. 1996), are at best of moderate spectral resolution, thereby limiting the analysis and interpretation (Liedahl et al. 1995). However high resolution spectra for such objects will soon become available from the AXAF and XMM satellites (Weisskopf 1988; Brinkman 1989), which will also provide observations for the coronal regions of late-type stars (Haisch & Schmitt 1996).

The modelling of Fe L-shell emission from all of the above astronomical objects requires reliable atomic data for the various processes occurring within the plasma (Brown et al. 1998), with photoionization and recombination being particularly important for the accretion-powered X-ray sources (Savin et al. 1997). In this paper we present highly accurate photoionization cross sections for Fe XVI, plus the associated recombination rate coefficients for Fe XVII.

Send offprint requests to: K.L. Bell (kl.bell@qub.ac.uk)

2. Photoionization of Fe XVI

2.1. Method

The Breit-Pauli R-matrix method (Scott & Burke 1980) has been used very successfully in a number of calculations in the last couple of years. For example, cross sections obtained using this method for both the $3p$-photoabsorption of Mn II (Donnelly et al. 1998a) and the photorecombination of Ar XIV (using Ar XIII photoionization cross sections) on storage rings (Zhang & Pradhan 1997), showed excellent agreement with experimental measurements. In addition, calculations on Fe XVIII and Fe XIX (Donnelly et al. 1998b, 1999) using this approach highlight the importance of relativistic effects in the study of highly ionized iron.

Using this method we initally represent the residual ion, Fe XVII, by the following 21 $LS\pi$ target states: $2s^2 2p^6\ ^1S$, $2s^2 2p^5 3s\ ^1P^o$, $^3P^o$, $2s^2 2p^5 3p\ ^1S$, ^3S, ^1P, ^3P, ^1D, ^3D, $2s^2 2p^5 3d\ ^1P^o$, $^3P^o$, $^1D^o$, $^3D^o$, $^1F^o$, $^3F^o$, $2s2p^6 3s\ ^1S$, ^3S, $2s2p^6 3p\ ^1P^o$, $^3P^o$, $2s2p^6 3d\ ^1D$ and ^3D. Each of these target states is represented using a configuration interaction type wavefunction, i.e.

$$\Phi\left(LS\right) = \sum_{n=1}^{M} a_n \phi_n\left(\alpha_n LS\right) \tag{1}$$

where the set $\{\phi_n\ n = 1, ..., M\}$ represents a set of configuration state functions which possess the same total $LS\pi$ symmetry and in the present calculation are constructed from the set of one-electron orbitals $\{1s, 2s, 2p, 3s, 3p, 3d, \overline{4p}, \overline{4d}\}$ whose radial parts are given by linear combinations of Slater-type orbitals

$$P_{nl}\left(r\right) = \sum_{j=1}^{k} c_{jnl} \left[\frac{\left(2\zeta_{jnl}\right)^{2I_{jnl}+1}}{\left(2I_{jnl}\right)!}\right]^{\frac{1}{2}} r^{I_{jnl}} e^{-\zeta_{jnl} r} \tag{2}$$

The $1s$, $2s$ and $2p$ orbitals are those calculated by Clementi & Roetti (1974) for the Hartree-Fock ground state of Fe XVII. The remaining orbitals are generated using the CIV3 code (Hibbert

Table 1. Radial function parameters for neon-like Fe XVII orbitals

Function	c_{jnl}	I_{jnl}	ζ_{jnl}	$\langle r \rangle$
$3s$	0.22832	1	19.39896	0.65601
	-1.06978	2	8.41790	
	1.53589	3	6.26321	
$3p$	0.60788	2	10.67797	0.63603
	-1.16899	3	5.85703	
$3d$	0.94583	3	6.34206	0.56972
	0.07100	3	3.54698	
$\overline{4p}$	8.57178	2	3.98622	0.60234
	-4.33646	3	3.95232	
	-5.17649	4	10.21242	
$\overline{4d}$	9.54153	3	3.48899	0.99710
	-10.00846	4	4.48185	

1975) in the following manner. The $3s$ and $3p$ orbitals are obtained by treating the exponents, ζ_{jnl}, as variational parameters in the minimization of the energies of the $2s^2 2p^5 3s\ ^3P^o$ and $2s^2 2p^5 3p\ ^3S$ states respectively while the powers of r, I_{jnl}, are kept fixed and the coefficients, c_{jnl}, are calculated subject to the orthonormality condition

$$\int_0^\infty P_{nl}(r)\, P_{n'l}(r)\, dr = \delta_{nn'} \tag{3}$$

The $3d$ orbital is obtained by optimizing on the $2s^2 2p^5 3d\ ^3P^o$ state but both exponents and coefficients are allowed to vary. Further valence shell correlation is introduced by using pseudo orbitals: a $\overline{4p}$ optimized on $2s^2 2p^5 3p\ ^3P$ using two configurations $[2s^2 2p^5 3p + 2s^2 2p^5 \overline{4p}]\ ^3P$ and a $\overline{4d}$ optimized on $2s^2 2p^5 3d\ ^3D^o$ using two configurations $[2s^2 2p^5 3d + 2s^2 2p^5 \overline{4d}]\ ^3D^o$. The resulting parameters for this orbital set are given in Table 1 along with the expectation value of the orbital radius, r. In Table 1, $3p$ and $3d$ refer to spectroscopic orbitals, while $\overline{4p}$ and $\overline{4d}$ refer to correlation orbitals. We note that we have not included *f* states, as their effects are expected to be negligible.

The set of configuration state functions of Eq. (1) is generated by allowing two electron replacement in the $2s^2 2p^6$ basis set with any other two electrons from the orbital set now available to us. This results in 825 configurations, too many configurations for the available computing resources. We therefore eliminated unimportant configurations using the following procedure. Examining the eigenvectors generated by the CIV3 computer code in determining the target state energies in LS-coupling, we only included those configurations which had an expansion coefficient, a_n (Eq. (1)), greater than 0.0075 for at least one of the target state wavefunctions. This procedure reduces the number of N-electron configurations to 171. Our choice of cut-off for a_n was made, noting that our wavefunctions must contain high accuracy. The recoupling method described by Scott & Burke (1980) is then employed to give the fine-structure energies and expansion coefficients. These energies and the major contributors to each target state are given in Table 2. The energies are compared with those obtained in the 825 configuration CIV3 calculation, the *ab initio* theoretical results of Bhatia & Doschek (1992), the adjusted theoretical results of Hibbert et al. (1993), and the experimental results compiled by NIST (obtained from the NIST atomic spectroscopic database at http://physics.nist.gov). The results obtained are highly satisfactory, although we note a significant difference when comparing the $2s$ hole states with those of Hibbert et al. We believe that this is due to the block adjustment used in the Hibbert et al. calculation enforced by the lack of experimental data. We note, however, that the present results agree well with the small amount of experimental data in this area and the results of Bhatia & Doschek. Of particular importance is the fact that no significant change occurs between the 825 and 171 configuration calculations for all states, suggesting that the method we have used in reducing the size of the problem is appropriate in this case.

To further confirm this assumption, however, we undertake the calculation of oscillator strengths for dipole allowed transitons between the target states using the CIV3 computer code for both the 171 and 825 configuration target state representations. The length form of these oscillator strengths are compared with the theoretical data of Hibbert et al. (1993) in Table 3. (Not all transitions are listed in the present publication and only those oscillator strengths greater than 0.0001 are included. The remaining oscillator strengths, however, are available from the authors on request). The results are again highly satisfactory particularly from the point of view of the small difference between the 171 and 825 configuration calculations. This, and the good agreement with Hibbert et al., indicate the satisfactory nature of the target state wavefunctions for the purposes of the present photoionization calculation.

Using basis states of the form

$$\begin{aligned}\psi_k(x_1, ..., x_{N+1}) = \\ \mathcal{A} \sum_{ij} c_{ijk} \overline{\Phi}_i(x_1, ..., x_N; \hat{\mathbf{r}}_{N+1}\sigma_{N+1}) \frac{1}{r_{N+1}} u_{ij}(r_{N+1}) \\ + \sum_j d_{jk} \chi_j(x_1, ..., x_{N+1})\end{aligned} \tag{4}$$

the $(N+1)$-electron wavefunction, Ψ, is represented by a configuration interaction type expansion,

$$\Psi = \sum_k A_{Ek} \psi_k \tag{5}$$

where A_{Ek} are energy dependent coefficients, u_{ij} are the radial functions of the continuum orbitals and $\overline{\Phi}_i$ are the channel functions obtained by coupling the target states Φ_i with the angular and spin functions of the continuum electrons to form states of total angular momentum and parity. $\mathcal{A}$ is the antisymmetrization operator which accounts for electron exchange between the target electrons and the free electron while χ_j represents the quadratically integrable (L^2) functions (or $(N+1)$- electron configurations) which are formed from the bound orbitals and are included to ensure completeness of the total wavefunction. In order to ensure that the Fe XVI and Fe XVII systems are balanced, the present calculation uses $(N+1)$-electron configurations that are obtained by adding one electron from the

Table 2. Target state energies (in a.u.) relative to the ground state of Fe XVII. Previous data are from the *ab initio* theoretical results of Bhatia & Doschek (1992), the adjusted theoretical results of Hibbert et al. (1993) and the experimental tabulations from the NIST atomic spectroscopic database

Target state	Present Calculation 171 Configurations	825 Configurations	Bhatia & Doschek	Hibbert et al.	NIST data	% purity	Other contributions
$2s^2 2p^6\ ^1S_o$	0.000000	0.000000	0.000000	0.000000	0.000000	99.9	
$2s^2 2p^5 3s\ ^3P^o_2$	26.722657	26.724064	26.680400	26.651746	26.648228	99.5	
$2s^2 2p^5 3s\ ^1P^o_1$	26.787769	26.791544	26.753216	26.721257	26.718305	55.9	43.6 $^3P^o_1$
$2s^2 2p^5 3s\ ^3P^o_0$	27.191088	27.238252	27.139847	27.113645	27.113384	99.5	
$2s^2 2p^5 3s\ ^3P^o_1$	27.227687	27.280069	27.187643	27.158483	27.156943	55.9	43.5 $^1P^o_1$
$2s^2 2p^5 3p\ ^3S_1$	27.831521	27.839219	27.789447	27.762164	27.760838	82.7	15.0 $^3P_1$
$2s^2 2p^5 3p\ ^3D_2$	27.981879	27.966026	27.924260	27.898089	27.889327	58.8	31.4 $^1D_2$ + 10.3 $^3P_2$
$2s^2 2p^5 3p\ ^3D_3$	28.034045	28.028556	27.980622	27.952733	27.948650	99.6	
$2s^2 2p^5 3p\ ^1P_1$	28.074408	28.065828	28.365987	27.994847	27.990158	51.1	25.3 $^3D_1$ + 20.3 $^3P_1$
$2s^2 2p^5 3p\ ^3P_2$	28.141916	28.130147	28.089090	28.059592	28.056817	67.9	31.3 $^1D_2$
$2s^2 2p^5 3p\ ^3P_0$	28.351409	28.357934	28.299387	28.268614	28.257709	93.1	
$2s^2 2p^5 3p\ ^3D_1$	28.424977	28.459728	28.480765	28.341264	28.333569	67.1	31.5 $^1P_1$
$2s^2 2p^5 3p\ ^3P_1$	28.535308	28.576882	28.023661	28.454261	28.452990	64.1	16.5 $^1P_1$ + 12.1 $^3S_1$
$2s^2 2p^5 3p\ ^1D_2$	28.549754	28.594278	28.496749	28.469680	28.466796	41.3	36.9 $^1D_2$ + 21.4 $^3P_2$
$2s^2 2p^5 3p\ ^1S_0$	29.045377	29.075944	29.082506	28.967609	28.944663	92.3	
$2s^2 2p^5 3d\ ^3P^o_0$	29.549222	29.537548	29.486051	29.449300	29.449094	99.2	
$2s^2 2p^5 3d\ ^3P^o_1$	29.588565	29.571876	29.524684	29.486219	29.490830	91.2	
$2s^2 2p^5 3d\ ^3P^o_2$	29.661916	29.650279	29.596952	29.553598	29.548787	71.6	20.4 $^3D^o_2$
$2s^2 2p^5 3d\ ^3F^o_4$	29.670605	29.657267	29.606379	29.560993	29.552022	99.7	
$2s^2 2p^5 3d\ ^3F^o_3$	29.686106	29.680389	29.627083	29.590846	29.580544	62.8	31.6 $^1F^o_3$
$2s^2 2p^5 3d\ ^1D^o_2$	29.750009	29.740130	30.119804	29.651587	29.643741	42.1	34.7 $^3D^o_2$ + 22.2 $^3F^o_2$
$2s^2 2p^5 3d\ ^3D^o_3$	29.791232	29.784840	29.736845	29.691860	29.683244	64.1	32.5 $^1F^o_3$
$2s^2 2p^5 3d\ ^3D^o_1$	29.962726	29.957084	29.907980	29.864400	29.853970	74.4	20.0 $^1P^o_1$
$2s^2 2p^5 3d\ ^3F^o_2$	30.150647	30.189992	30.083950	30.048429	30.043786	62.6	30.1 $^1D^o_2$
$2s^2 2p^5 3d\ ^3D^o_2$	30.181190	30.221125	29.689427	30.075862	30.080829	50.9	26.1 $^3P^o_2$ + 20.4 $^1D^o_2$
$2s^2 2p^5 3d\ ^1F^o_3$	30.201667	30.245864	30.142832	30.097423	30.098645	35.5	33.9 $^3F^o_3$ + 30.2 $^3D^o_3$
$2s^2 2p^5 3d\ ^1P^o_1$	30.461362	30.494562	30.432778	30.369700	30.345142	78.1	17.5 $^3D^o_1$
$2s2p^6 3s\ ^3S_1$	31.753226	31.699164	31.674396	31.205595	-	98.7	
$2s2p^6 3s\ ^1S_0$	31.950981	31.910476	31.919321	31.426969	-	99.6	
$2s2p^6 3p\ ^3P^o_0$	32.988470	31.906408	32.878770	32.317808	-	99.3	
$2s2p^6 3p\ ^3P^o_1$	33.005639	32.923495	32.896585	32.336088	32.800547	87.4	11.8 $^1P^o_1$
$2s2p^6 3p\ ^3P^o_2$	33.094295	33.011783	32.981410	32.420284	32.961841	99.3	
$2s2p^6 3p\ ^1P^o_1$	33.157578	33.075209	32.051837	32.488552	-	87.5	11.9 $^3P^o_1$
$2s2p^6 3d\ ^3D_1$	34.662611	34.582281	34.539337	33.926338	-	99.9	
$2s2p^6 3d\ ^3D_2$	34.671642	34.591909	34.548482	33.932603	-	99.5	
$2s2p^6 3d\ ^3D_3$	34.687088	34.608001	34.564201	33.942422	-	99.9	
$2s2p^6 3d\ ^1D_2$	34.881021	34.772529	34.742536	34.124670	-	99.6	

orbital set to the 171 configurations used in the target state representation. Effectively, we are thus treating Fe XVI as a bound state of the (Fe XVII +e$^-$) system, while the motion and energy of the free electron is represented by the set of continuum orbitals. Twenty-five such orbitals were used for each value of $l \leq 6$ and an R-matrix radius of 9.2 Ryd. was employed.

Selection rules indicate that only two transitions need concern us in the present calculation: $\frac{1}{2}^e \rightarrow \frac{1}{2}^o$ and $\frac{1}{2}^e \rightarrow \frac{3}{2}^o$. Hamiltonian matrices are calculated for the three symmetries involved in these transitions where all the $LS\pi$ symmetries which contribute to these are included. An indication of the accuracy of the approach thus far used is given in the calculation of the $2s^2 2p^6 3s\ ^2S_{1/2}$ Fe XVI bound state wavefunction which provides a value for the ionization energy. A value of 36.12 Ryd. is obtained which is in excellent agreement with the value of 36.18 Ryd calculated by Verner et al. (1993) and the value of 35.96 Ryd tabulated by NIST.

Pradhan & Zhang (1997) recently performed investigations into the effect of the inclusion of radiation damping on photoionization cross sections and recombination rates. The effect on larger resonances was minimal and while weak resonances may be damped out, the omission of damping is unlikely to cause serious inaccuracies in the photoionization cross sections.

Table 3. Oscillator Strengths greater than 0.0001 for dipole allowed transitions between states of Fe XVII. Comparison is made with the results of Hibbert et al. (1993)

Transition	171 config.	825 configs	Hibbert et al.
$2s^2 2p^6 \rightarrow 2s^2 2p^5 3s$			
$^1S_0 \rightarrow {}^1P_1^o$	0.1252	0.1232	0.1218
$^1S_0 \rightarrow {}^3P_1^o$	0.0924	0.0949	0.1015
$2s^2 2p^6 \rightarrow 2s^2 2p^5 3d$			
$^1S_0 \rightarrow {}^3P_1^o$	0.0098	0.0096	0.0106
$^1S_0 \rightarrow {}^3D_1^o$	0.7107	0.7034	0.6042
$^1S_0 \rightarrow {}^1P_1^o$	2.2308	2.2705	2.3525
$2s^2 2p^5 3s \rightarrow 2s^2 2p^5 3p$			
$^3P_2^o \rightarrow {}^3S_1$	0.0516	0.0520	0.0500
$^3P_2^o \rightarrow {}^3D_2$	0.0500	0.0508	0.0506
$^3P_2^o \rightarrow {}^3D_3$	0.1658	0.1627	0.1615
$^3P_2^o \rightarrow {}^1P_1$	0.0040	0.0032	0.0039
$^3P_2^o \rightarrow {}^3P_2$	0.0739	0.0693	0.0694
$^3P_2^o \rightarrow {}^3P_1$	0.0051	0.0044	0.0051
$^3P_2^o \rightarrow {}^1D_2$	0.0011	0.0009	0.0011
$^1P_1^o \rightarrow {}^3S_1$	0.0040	0.0032	0.0038
$^1P_1^o \rightarrow {}^3D_2$	0.0999	0.0946	0.0946
$^1P_1^o \rightarrow {}^1P_1$	0.1089	0.1073	0.1059
$^1P_1^o \rightarrow {}^3P_2$	0.0912	0.0918	0.0911
$^1P_1^o \rightarrow {}^3P_0$	0.0359	0.0349	0.0341
$^1P_1^o \rightarrow {}^3D_1$	0.0004	0.0004	0.0004
$^1P_1^o \rightarrow {}^1D_2$	0.0016	0.0010	0.0014
$^1P_1^o \rightarrow {}^1S_0$	0.0235	0.0235	0.0247
$^3P_0^o \rightarrow {}^3S_1$	0.0020	0.0018	0.0022
$^3P_0^o \rightarrow {}^1P_1$	0.0004	0.0004	0.0007
$^3P_0^o \rightarrow {}^3D_1$	0.1222	0.1250	0.1279
$^3P_0^o \rightarrow {}^3P_1$	0.2230	0.2138	0.2088
$^3P_1^o \rightarrow {}^3S_1$	0.0009	0.0008	0.0010
$^3P_1^o \rightarrow {}^3P_2$	0.0011	0.0010	0.0015
$^3P_1^o \rightarrow {}^3P_0$	0.0095	0.0090	0.0096
$^3P_1^o \rightarrow {}^3D_1$	0.0659	0.0633	0.0621
$^3P_1^o \rightarrow {}^3P_1$	0.0404	0.0411	0.0416
$^3P_1^o \rightarrow {}^1D_2$	0.1996	0.1949	0.1936
$^3P_1^o \rightarrow {}^1S_0$	0.0428	0.0426	0.0434
$2s^2 2p^3 3p \rightarrow 2s^2 2p^5 3d$			
$^3S_1 \rightarrow {}^3P_0^o$	0.0416	0.0416	0.0401
$^3S_1 \rightarrow {}^3P_1^o$	0.1025	0.1013	0.0981
$^3S_1 \rightarrow {}^3P_2^o$	0.0936	0.0882	0.0874
$^3S_1 \rightarrow {}^1D_2^o$	0.0024	0.0046	0.0050
$^3S_1 \rightarrow {}^3D_1^o$	0.0001	0.0003	0.0004
$^3S_1 \rightarrow {}^3F_2^o$	0.0002	0.0002	0.0003
$^3S_1 \rightarrow {}^3D_2^o$	0.0010	0.0007	0.0007
$^3D_2 \rightarrow {}^3P_1^o$	0.0056	0.0059	0.0057
$^3D_2 \rightarrow {}^3P_2^o$	0.0120	0.0112	0.0090
$^3D_2 \rightarrow {}^3F_3^o$	0.1730	0.1696	0.1668
$^3D_2 \rightarrow {}^1D_2^o$	0.0495	0.0498	0.0503
$^3D_2 \rightarrow {}^3D_3^o$	0.0011	0.0009	0.0015
$^3D_2 \rightarrow {}^3D_1^o$	0.0034	0.0033	0.0035
$^3D_2 \rightarrow {}^3F_2^o$	0.0004	0.0004	0.0007
$^3D_2 \rightarrow {}^3D_2^o$	0.0012	0.0013	0.0016
$^3D_2 \rightarrow {}^1P_1^o$	0.0001	0.0001	0.0001
$^3D_3 \rightarrow {}^3P_2^o$	0.0031	0.0030	0.0029
$^3D_3 \rightarrow {}^3F_4^o$	0.1795	0.1756	0.1724
$^3D_3 \rightarrow {}^3F_3^o$	0.0199	0.0200	0.0205
$^3D_3 \rightarrow {}^1D_2^o$	0.0016	0.0017	0.0019
$^3D_3 \rightarrow {}^3D_3^o$	0.0304	0.0292	0.0276
$^3D_3 \rightarrow {}^3D_2^o$	0.0010	0.0009	0.0009
$^3D_3 \rightarrow {}^1F_3^o$	0.0009	0.0009	0.0011
$^1P_1 \rightarrow {}^3P_0^o$	0.0016	0.0012	0.0015
$^1P_1 \rightarrow {}^3P_1^o$	0.0010	0.0006	0.0006
$^1P_1 \rightarrow {}^3P_2^o$	0.0203	0.0156	0.0218
$^1P_1 \rightarrow {}^1D_2^o$	0.1522	0.1594	0.1479
$^1P_1 \rightarrow {}^3D_1^o$	0.0674	0.0663	0.0648
$^1P_1 \rightarrow {}^3D_2^o$	0.0003	0.0004	0.0004
$^1P_1 \rightarrow {}^1P_1^o$	0.0097	0.0094	0.0103
$^3P_2 \rightarrow {}^3P_1^o$	0.0103	0.0100	0.0098
$^3P_2 \rightarrow {}^3P_2^o$	0.0541	0.0525	0.0847
$^3P_2 \rightarrow {}^3F_3^o$	0.0021	0.0024	0.0017
$^3P_2 \rightarrow {}^1D_2^o$	0.0002	0.0001	0.0000
$^3P_2 \rightarrow {}^3D_3^o$	0.1619	0.1593	0.1589
$^3P_2 \rightarrow {}^3F_2^o$	0.0003	0.0002	0.0002
$^3P_2 \rightarrow {}^3D_2^o$	0.0046	0.0042	0.0052
$^3P_2 \rightarrow {}^1F_3^o$	0.0001	0.0001	0.0002
$^3P_2 \rightarrow {}^1P_1^o$	0.0002	0.0001	0.0002
$^3P_0 \rightarrow {}^3P_1^o$	0.0089	0.0089	0.0104
$^3P_0 \rightarrow {}^3D_1^o$	0.2056	0.2026	0.2015
$^3P_0 \rightarrow {}^1P_1^o$	0.0159	0.0163	0.0144
$^3D_1 \rightarrow {}^3P_2^o$	0.0003	0.0003	0.0005
$^3D_1 \rightarrow {}^3D_1^o$	0.0022	0.0020	0.0021
$^3D_1 \rightarrow {}^3F_2^o$	0.2049	0.2078	0.2022
$^3D_1 \rightarrow {}^3D_2^o$	0.0002	0.0001	0.0001
$^3D_1 \rightarrow {}^1P_1^o$	0.0450	0.0436	0.0426
$^3P_1 \rightarrow {}^3P_0^o$	0.0014	0.0012	0.0014
$^3P_1 \rightarrow {}^3P_1^o$	0.0012	0.0010	0.0012
$^3P_1 \rightarrow {}^3P_2^o$	0.0004	0.0003	0.0006
$^3P_1 \rightarrow {}^3F_2^o$	0.0022	0.0026	0.0043
$^3P_1 \rightarrow {}^3D_1^o$	0.0025	0.0024	0.0031
$^3P_1 \rightarrow {}^3D_2^o$	0.2010	0.2048	0.1945
$^3P_1 \rightarrow {}^1P_1^o$	0.0246	0.0251	0.0253
$^1D_2 \rightarrow {}^3P_1^o$	0.0005	0.0005	0.0005
$^1D_2 \rightarrow {}^3P_2^o$	0.0009	0.0008	0.0011
$^1D_2 \rightarrow {}^3D_3^o$	0.0001	0.0002	0.0003
$^1D_2 \rightarrow {}^3D_1^o$	0.0007	0.0006	0.0006
$^1D_2 \rightarrow {}^3F_2^o$	0.0202	0.0195	0.0178
$^1D_2 \rightarrow {}^3D_2^o$	0.0124	0.0125	0.0135
$^1D_2 \rightarrow {}^1F_3^o$	0.1988	0.1948	0.1921
$^1D_2 \rightarrow {}^1P_1^o$	0.0011	0.0011	0.0010
$^1S_0 \rightarrow {}^3D_1^o$	0.0049	0.0053	0.0055
$^1S_0 \rightarrow {}^1P_1^o$	0.1775	0.1740	0.1777

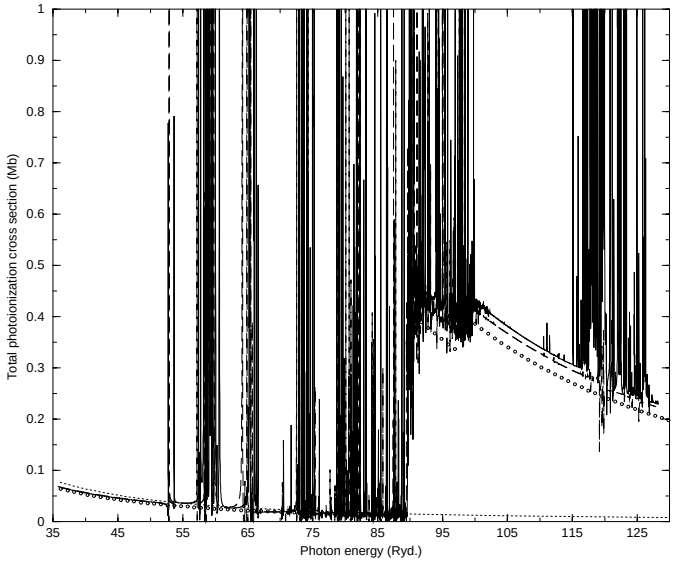

Fig. 1. Total photoionization cross sections for the photoionization of the Fe XVI ground state (solid curve) compared with the present calculation performed in LS-coupling (dashed curve), the Opacity Project calculation (dotted curve) and the work of Verner et al. (circles)

Radiation damping of autoionization resonances has thus been omitted in the present investigation.

2.2. Results and discussion

Total photoionization cross sections are calculated in the $30 \rightarrow 130$ Ryd. photon energy range using a step size of 1×10^{-2} Ryd. The results are presented in Fig. 1. We note the sharp jump in the cross section at photon energies of 89.54 Ryd and 99.64 Ryd, which correspond to the $2p$ and $2s$ thresholds respectively, and the extensive resonance structure included due to the high resolution. A comparison with the Opacity Project LS-coupled calculation and the data of Verner et al. (1993) is also provided in Fig. 1. The agreement with the work of Verner et al. is highly satisfactory, particularly regarding the increase of the magnitude of the background cross section at the threshold positions. Agreement with the Opacity Project data is also highly satisfactory although it is noted that $2p$ and $2s$ photoionization was not included in that calculation and thus comparison above the $2p$ threshold is not meaningful. In addition we have shifted the Opacity Project results by 3 Ryd in order to match the positions of the $3s$ threshold with that of the present work. No shift was required for the present work or that of Verner et al.

Previous calculations for other ions of iron (Donnelly et al. 1998b, 1999) showed that the introduction of relativistic effects caused a significant change in the magnitude of the background cross section, due to the increase in the amount of configuration interaction occurring in the target state representation through the inclusion of the spin orbit operator. To investigate the effect of including relativity in the present case, we calculate the LS-coupled cross sections for the present scenario. The results are also provided in Fig. 1. In the region of $3s$ photoionization, very little difference is observed between the two calculations, which is consistent with the observed purity of the target ground state in both coupling schemes. Significant mixing between the $2s^2 2p^5 3s\ ^1P^o_1$ and $^3P^o_1$ target states produces a slight increase in the background cross section shortly following the $2p$ ionization threshold. (The question of whether or not relativistic effects increase or decrease the background cross section is dependent solely on the magnitude of the partial cross sections involved). The mixing in the remaining target states, however, has little effect on the magnitude of the total cross section, due to the relatively small magnitude of the partial cross sections for these target states. This can be seen in Fig. 2, which illustrates the partial cross sections for photoionization to each of the target states. The $2s2p^6 3p$ and $2s2p^6 3d$ partial cross sections are omitted due to their small magnitude. All partial cross sections, however, are available from the authors on request.

3. Recombination rates for Fe XVII

3.1. Method

The recombination rate coefficient, α_{ji}, for electrons combining with Fe XVII in state i to form Fe XVI in state j is related to the partial photoionization cross section σ_{ij} by the Milne relation (Milne 1924)

$$\alpha_{ji}(T) = \frac{\omega_j}{\omega_i}\sqrt{\frac{2}{\pi}}\frac{1}{c^2(mkT)^{\frac{3}{2}}}\times \int_{I_{ji}}^{\infty}(h\nu)^2\sigma_{ij}(h\nu)\exp\left[-\frac{h\nu - I_{ji}}{kT}\right]dh\nu \qquad (6)$$

where: I_{ji} is the ionization potential from the jth state of Fe XVI to the ith state of Fe XVII; T is the temperature of the free electrons, and m is the electron mass; ω_i and ω_j are the statistical weights of the respective ionic states. We note that the total recombination coefficient requires the addition of the contributions of recombination to excited states of the product ion.

3.2. Results and discussion

The set of partial cross sections obtained in Sect. 2 are utilized to obtain the recombination rates for the process of recombination to each of the Fe XVII target states forming the ground state of Fe XVI. The results for the target states which contribute significantly to the total photoionization cross section (as illustrated in Fig. 2) are given in Table 4 for a variety of temperatures. (The rates for the remaining target states are available from the authors). We note, however, that due to the presence of numerous autoionization resonances the recombination rates calculated in this procedure also include low-energy dielectronic recombination in addition to radiative recombination.

4. Summary

To summarize, we have completed an extensive calculation of the photoionization of the ground state of Fe XVI and presented both total and partial cross sections, the latter of which have

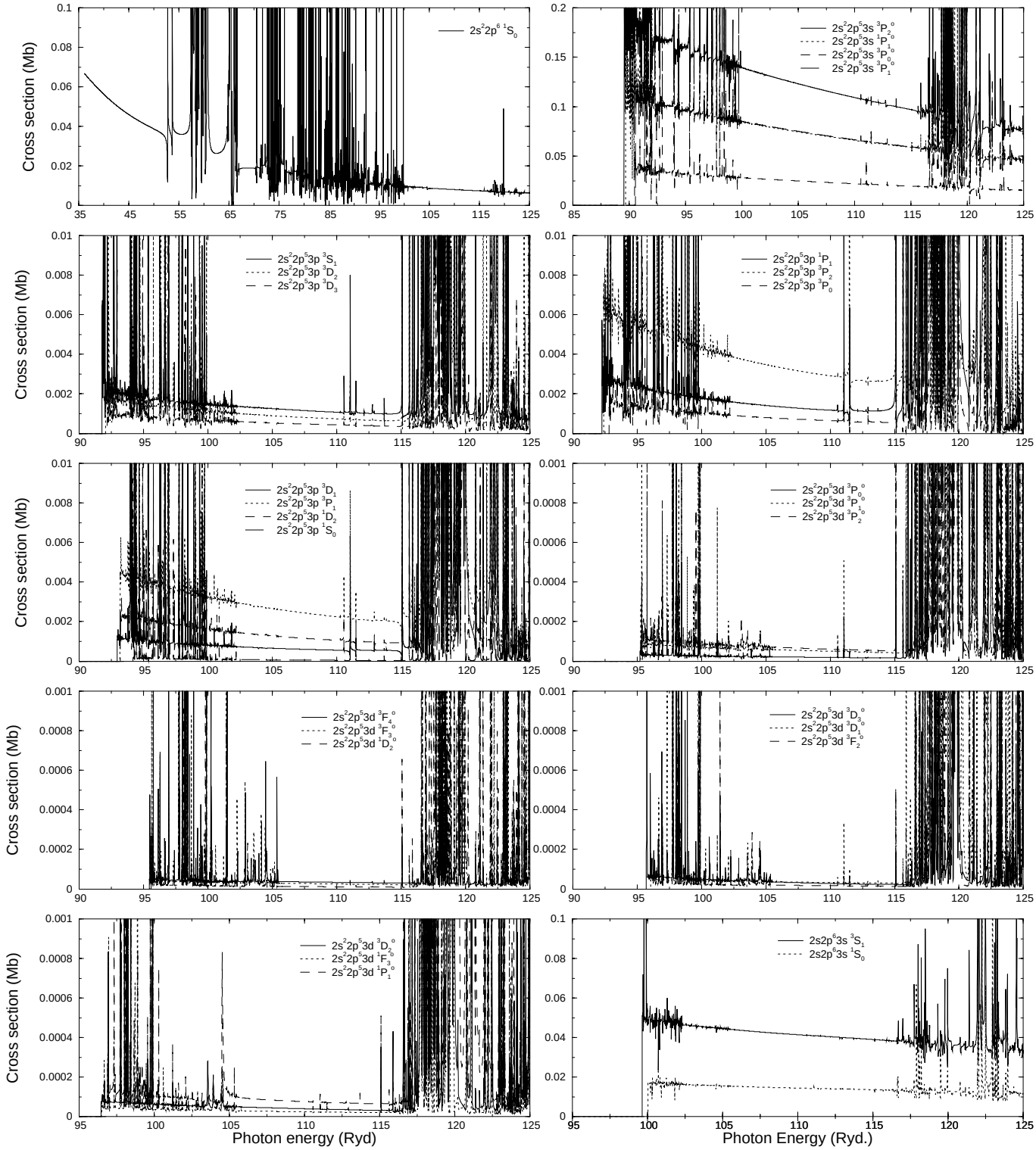

Fig. 2. Partial photoionization cross sections for the photoionization of the ground state of Fe XVI with the residual ion left in one of the target states

been used in the development of a set of recombination rates. Relativistic effects have been considered, and are seen to have a noticeable effect on the background cross section above the $2p$ threshold. More extensive resonance structure is observed than in previous calculations, but otherwise agreement with other studies is highly favourable.

Table 4. Recombination rate coefficients for the recombination of states of Fe XVII with an electron to form Fe XVI in its ground state

Temperature	Recombination rates ($cm^3\ s^{-1}$) from ...						
(K)	$2s^2 2p^6\ ^1S_0$	$2s^2 2p^5 3s\ ^3P^o_2$	$2s^2 2p^5 3s\ ^1P^o_1$	$2s^2 2p^5 3s\ ^3P^o_0$	$2s^2 2p^5 3s\ ^3P^o_1$	$2s 2p^6 3s\ ^3S_1$	$2s 2p^6 3s\ ^1S_0$
5×10^4	1.02×10^{-12}	4.15×10^{-12}	4.35×10^{-12}	3.76×10^{-12}	3.61×10^{-12}	2.12×10^{-12}	1.96×10^{-12}
6×10^4	9.32×10^{-13}	3.77×10^{-12}	3.96×10^{-12}	3.45×10^{-12}	3.33×10^{-12}	1.92×10^{-12}	1.80×10^{-12}
7×10^4	8.63×10^{-13}	3.48×10^{-12}	3.66×10^{-12}	3.20×10^{-12}	3.11×10^{-12}	1.76×10^{-12}	1.66×10^{-12}
8×10^4	8.08×10^{-13}	3.24×10^{-12}	3.41×10^{-12}	3.01×10^{-12}	2.94×10^{-12}	1.64×10^{-12}	1.56×10^{-12}
9×10^4	7.62×10^{-13}	3.04×10^{-12}	3.20×10^{-12}	2.84×10^{-12}	2.79×10^{-12}	1.54×10^{-12}	1.47×10^{-12}
1×10^5	7.24×10^{-13}	2.87×10^{-12}	3.03×10^{-12}	2.70×10^{-12}	2.67×10^{-12}	1.45×10^{-12}	1.40×10^{-12}
2×10^5	5.14×10^{-13}	1.95×10^{-12}	2.08×10^{-12}	1.91×10^{-12}	1.94×10^{-12}	9.96×10^{-13}	9.93×10^{-13}
3×10^5	4.24×10^{-13}	1.56×10^{-12}	1.66×10^{-12}	1.55×10^{-12}	1.59×10^{-12}	8.04×10^{-13}	8.13×10^{-13}
4×10^5	3.89×10^{-13}	1.33×10^{-12}	1.42×10^{-12}	1.33×10^{-12}	1.37×10^{-12}	6.92×10^{-13}	7.06×10^{-13}
5×10^5	4.30×10^{-13}	1.17×10^{-12}	1.25×10^{-12}	1.18×10^{-12}	1.22×10^{-12}	6.18×10^{-13}	6.33×10^{-13}
6×10^5	5.66×10^{-13}	1.06×10^{-12}	1.13×10^{-12}	1.07×10^{-12}	1.11×10^{-12}	5.64×10^{-13}	5.80×10^{-13}
7×10^5	7.92×10^{-13}	9.69×10^{-13}	1.03×10^{-12}	9.88×10^{-13}	1.02×10^{-12}	5.22×10^{-13}	5.38×10^{-13}
8×10^5	1.08×10^{-12}	9.00×10^{-13}	9.59×10^{-13}	9.20×10^{-13}	9.51×10^{-13}	4.89×10^{-13}	5.04×10^{-13}
9×10^5	1.41×10^{-12}	8.42×10^{-13}	8.97×10^{-13}	8.63×10^{-13}	8.92×10^{-13}	4.62×10^{-13}	4.76×10^{-13}
1×10^6	1.76×10^{-12}	7.94×10^{-13}	8.45×10^{-13}	8.15×10^{-13}	8.43×10^{-13}	4.38×10^{-13}	4.52×10^{-13}
2×10^6	3.93×10^{-12}	5.28×10^{-13}	5.54×10^{-13}	5.40×10^{-13}	5.66×10^{-13}	2.93×10^{-13}	3.00×10^{-13}
3×10^6	4.15×10^{-12}	3.93×10^{-13}	4.10×10^{-13}	4.00×10^{-13}	4.24×10^{-13}	2.13×10^{-13}	2.17×10^{-13}
4×10^6	3.80×10^{-12}	3.07×10^{-13}	3.19×10^{-13}	3.11×10^{-13}	3.32×10^{-13}	1.63×10^{-13}	1.65×10^{-13}
5×10^6	3.35×10^{-12}	2.48×10^{-13}	2.56×10^{-13}	2.50×10^{-13}	2.68×10^{-13}	1.29×10^{-13}	1.31×10^{-13}
6×10^6	2.93×10^{-12}	2.05×10^{-13}	2.12×10^{-13}	2.06×10^{-13}	2.22×10^{-13}	1.06×10^{-13}	1.07×10^{-13}
7×10^6	2.57×10^{-12}	1.73×10^{-13}	1.79×10^{-13}	1.74×10^{-13}	1.88×10^{-13}	8.84×10^{-14}	8.89×10^{-14}
8×10^6	2.28×10^{-12}	1.49×10^{-13}	1.53×10^{-13}	1.49×10^{-13}	1.61×10^{-13}	7.53×10^{-14}	7.57×10^{-14}
9×10^6	2.02×10^{-12}	1.30×10^{-13}	1.33×10^{-13}	1.29×10^{-13}	1.41×10^{-13}	6.51×10^{-14}	6.54×10^{-14}
1×10^7	1.81×10^{-12}	1.14×10^{-13}	1.17×10^{-13}	1.14×10^{-13}	1.24×10^{-13}	5.70×10^{-14}	5.72×10^{-14}

Acknowledgements. This work was supported by PPARC under grant PPA/G/O/1997/00693. All R-matrix calculations were performed on the CRAY J932 located at the Rutherford Appleton Laboratory.

References

Audley M.D., Kelley R.L., Boldt E.A., et al., 1996, ApJ 457, 397
Bhatia A.K., Doschek G.A., 1992, At. Data. Nucl. Data Tables 52, 1
Brinkman A.C., 1989, In: Hailey C.J., Siegmund O.H.W. (eds.) Proc. SPIE, EUV, X-Ray and Gamma-Ray Instrumentation for Astronomy and Astrophysics. 1159, 495
Brown G.V., Beiersdorfer P., Liedahl D.A., et al., 1998, ApJ 502, 1015
Clementi E., Roetti C., 1974, At. Data Nucl. Data Tables 14, 177
Donnelly D., Bell K.L., Hibbert A., 1998a, J. Phys. B: At. Mol. Opt. Phys. 31, L971
Donnelly D., Bell K.L., Keenan F.P., 1998b, A&AS 133, 249
Donnelly D., Bell K.L., Keenan F.P., 1999, MNRAS, in press
Haisch B., Schmitt J.H.M.M., 1996, PASP 108, 113
Hibbert A., 1975, Comput. Phys. Commun. 9, 141
Hibbert A., Le Dourneuf M., Mohan M., 1993, At. Data Nucl. Data Tables 53, 23
Keenan F.P., 1996, Space Sci. Rev. 75, 537
Liedahl D.A., Osterheld A.L., Goldstein W.H., 1995, ApJ 438, L115
Milne E.A., 1924, Phil. Mag. 47, 209
Phillips K.J.H., Leibacher J.W., Wolfson C.J., et al., 1982, ApJ 256, 774
Pradhan A.K., Zhang H.L., 1997, J. Phys. B: At. Mol. Opt. Phys. 30, L571
Savin D.W., Bartsch T., Chen M.H., et al., 1997, ApJ 489, L115
Scott N.S., Burke P.G., 1980, J. Phys. B: At. Mol. Phys. 13, 4299
Verner D.A., Yakovlev D.G., Band I.M, Trzhaskovskaya M.B., 1993, At. Data Nucl. Data Tables 55, 233
Weisskopf M.C., 1988, Space Sci. Rev. 47, 47
Yaqoob T., Serlemitsos P.J., Ptak A., et al., 1995, ApJ 455, 508
Zhang H.L., Pradhan A.K., 1997, Phys. Rev. Lett. 78, 195